Letter | Editors' Suggestion

Thermoelectric signatures of order-parameter symmetries in iron-based superconducting tunnel junctions

Claudio Guarcello,[1,2,*] Alessandro Braggio,[3,†] Francesco Giazotto,[3,‡] and Roberta Citro[1,2,4,§]

[1]*Dipartimento di Fisica "E.R. Caianiello," Università di Salerno, Via Giovanni Paolo II, 132, I-84084 Fisciano (Salerno), Italy*
[2]*INFN, Sezione di Napoli Gruppo Collegato di Salerno, Complesso Universitario di Monte S. Angelo, I-80126 Napoli, Italy*
[3]*NEST, Istituto Nanoscienze-CNR and Scuola Normale Superiore, Piazza San Silvestro 12, I-56127 Pisa, Italy*
[4]*CNR-SPIN c/o Universitá degli Studi di Salerno, I-84084 Fisciano (Salerno), Italy*

(Received 11 March 2023; revised 26 August 2023; accepted 29 August 2023; published 29 September 2023)

Thermoelectrical properties are frequently used to characterize materials and endow the free energy from wasted heat with useful purposes. Here, we show that linear thermoelectric effects in tunnel junctions with Fe-based superconductors not only address the dominance between particle and hole states but also even provide information about the superconducting order-parameter symmetry. In particular, we observe that nodal order parameters present a maximal thermoelectric effect at lower temperatures than for nodeless cases. Furthermore, we show also that superconducting tunnel junctions between Fe-based and BCS superconductors could provide a thermoelectric efficiency ZT exceeding 6 with a linear Seebeck coefficient around $S \approx 800\ \mu V/K$ at a few kelvins. These results pave the way to developing novel thermoelectric machines based on multiband superconductors.

DOI: 10.1103/PhysRevB.108.L100511

Introduction. Physical systems based on hybrid superconducting junctions have demonstrated a great potential for energy management issues [1–4]. Recently, they have also attracted interest for their unexpectedly good thermoelectric (TE) performance [5–12], finding also a role in different quantum technology applications [13–15]. In a two-terminal system, a necessary condition for thermoelectricity in the linear regime, i.e., for a small voltage δV and a small temperature bias δT, is breaking of the particle-hole (PH) symmetry. A sizable linear TE effect, much larger than that commonly found in metallic structures, has been recently reported in superconductor (SC)–ferromagnet tunnel junctions (TJs) [5,6,16], due to the spin-dependent effective breaking of PH symmetry.

Here, we show a robust linear TE effect in hybrid superconducting junctions with a multiband SC, namely, an Fe-based SC (FeSC). Our results, beyond proving a linear TE effect with unconventional SCs, establish TE phenomena as a potential probe of the superconducting order-parameter symmetries. In fact, one of the central problems for unconventional SCs is the nature of the pairing mechanism, which is tightly connected to the order-parameter symmetries [17–20]. Pairing symmetry is known to be d wave in cuprates but is still unresolved for the FeSCs. They are unique among unconventional SCs, since different ordering phenomena are present in a multiorbital scenario [21–23]. It was first theoretically predicted that FeAs-based high-temperature SCs have a sign change of the order parameter on the Fermi surface [21]. Experimental evidence for FeSCs seems to be favorable to $s_\pm$ pairing, implying that the electronlike and holelike bands both develop an s-wave superconducting state with opposite sign of the order parameter [21,24]. Point contact Andreev reflection spectroscopy has also been applied to FeSCs to probe the order-parameter symmetry [25,26]. However, the results of these studies are not completely conclusive due to the complexity of the Andreev reflection spectra of a normal-metal/multiband-SC interface. Notably, bulk thermoelectrical measurements of FeSCs have been reported for the normal state [27], although the analysis is quite intricate due to the competition of different mechanisms, such as phonon-drag [28] and magnon-drag phenomena [29], in a multiband setting. The linear TE properties of a TJ between an FeSC and a normal metal allow the strong intrinsic PH asymmetry in the FeSC density of states (DoS) to be identified in a quite direct way, *also for* the superconducting phase. We will also potentially discriminate between different order-parameter symmetries. Furthermore, if the normal metal is replaced by a Bardeen-Cooper-Schrieffer (BCS) SC, we observe also astounding TE figures of merit, which may be relevant for energy-harvesting applications and quantum technologies [14,15,30,31].

Thermoelectrical transport. In order to address the physics of the FeSC, we focus on the linear TE properties of a TJ between an FeSC and a normal metal (or a SC); see Fig. 1(a). The linear response coefficients of charge (I) and heat ($\dot{Q}$) currents can be expressed in terms of the Onsager matrix [32]

$$\begin{pmatrix} I \\ \dot{Q} \end{pmatrix} = \begin{pmatrix} \sigma & \alpha \\ \alpha & \kappa T \end{pmatrix} \begin{pmatrix} \delta V \\ \delta T/T \end{pmatrix}, \tag{1}$$

where we assumed that time-reversal symmetry is satisfied and that there is a small voltage (temperature) bias δV (δT). Here, α is the TE coefficient, while σ and κ are the electric

*Corresponding author: cguarcello@unisa.it
†alessandro.braggio@nano.cnr.it
‡francesco.giazotto@nano.cnr.it
§rocitro@unisa.it

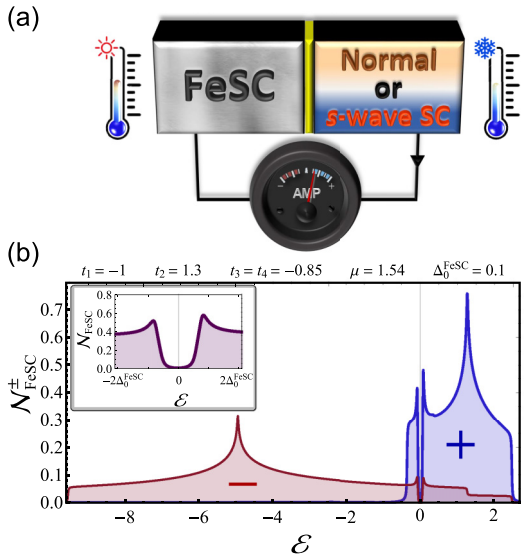

FIG. 1. (a) Cartoon of the thermally biased TJ formed by an FeSC and a normal or s-wave superconducting electrode. (b) Electronlike (+, blue curve) and holelike (−, red curve) band contributions to the DoS, $\mathcal{N}^{\pm}_{\rm FeSC}(\varepsilon)$; see Eq. (4). The hopping parameters, in units of $|t_1|$, are $(t_1, t_2, t_3, t_4) = (-1, 1.3, -0.85, -0.85)$. The chemical potential is taken at half filling $\mu = 1.54$, and the gap size is assumed to be $\Delta_0^{\rm FeSC} = 0.1$. The inset shows a magnification of the total DoS, $\mathcal{N}_{\rm FeSC}(\varepsilon)$, in the energy range $|\varepsilon| \leqslant 2\Delta_0^{\rm FeSC}$.

and thermal conductances, respectively. At the lowest order of tunneling, it is easy to express those linear coefficients as

$$\begin{pmatrix}\sigma\\ \alpha\\ \kappa\end{pmatrix} = \frac{G_T}{e}\int_{-\infty}^{\infty}\begin{pmatrix}e\\ \varepsilon\\ \varepsilon^2/eT\end{pmatrix}\frac{\mathcal{N}_L(\varepsilon)\mathcal{N}_R(\varepsilon)d\varepsilon}{4k_{\rm B}T\cosh^2(\varepsilon/2k_{\rm B}T)} \tag{2}$$

in terms of the lead DoS, $\mathcal{N}_j(\epsilon)$ with $j = L, R$, where G_T is the normal-state conductance of the junction, $-e$ is the electron charge, and $k_{\rm B}$ is the Boltzmann constant. In our analysis, we take into account two different cases, i.e., a junction formed by an FeSC tunnel coupled with a normal lead, i.e., with $\mathcal{N}_R(\epsilon) = 1$ being the energy-independent normalized DoS in Eq. (2), or alternatively with an s-wave SC, with $\mathcal{N}_R(\epsilon) = |{\rm Re}[\frac{\epsilon+i\Gamma}{\sqrt{(\epsilon+i\Gamma)^2-\Delta^2(T)}}]|$, where $\Gamma = \gamma\Delta_0$ is the phenomenological Dynes parameter [33], $\Delta_0 = 1.764k_{\rm B}T_c$, and T_c is the critical temperature of the BCS SC. In this case, it is also implicitly assumed that the Josephson coupling [34,35] between the two superconducting leads is strongly suppressed [36]. However, let us point out that most of the results shown in the following, particularly those in which we will look at the effect of the order-parameter symmetry on the TE response, are obtained by considering an FeSC-I-N junction, where the Josephson effect is not even present.

To calculate the DoS of an FeSC, we rely on the two-orbital, four-band tight-binding approach given by Raghu *et al.* [37], which is the minimal model [38]. The diagonalization of this tight-binding Hamiltonian model leads to eigenvalues that can be written in a compact form as

$$\varepsilon^d_{\mathbf{k}\pm} = \sqrt{\left(\varepsilon^0_{\mathbf{k}\pm}\right)^2 + |\vec{d}_{\mathbf{k},g}|^2}. \tag{3}$$

Here, $\varepsilon^0_{\mathbf{k}\pm} = \xi_{\mathbf{k}+} - \mu \pm \sqrt{\xi^2_{\mathbf{k}xy} + \xi^2_{\mathbf{k}-}}$, μ is the chemical potential, and $\vec{d}_{\mathbf{k},g} = (0, 0, s_{x^2y^2})$, where $s_{x^2y^2} \equiv s_\pm = \Delta_0^{\rm FeSC}\cos k_x \cos k_y$, $\Delta_0^{\rm FeSC}$ is the gap size, and $|\vec{d}_{\mathbf{k}}|^2$ represents the effective amplitude of the pairing interactions [39]. For the explicit expressions of $\xi_{\mathbf{k}\pm}$ and $\xi_{\mathbf{k}xy}$ we refer the reader to the Supplemental Material [40]. We adopted the $s_\pm$-wave state, which is the mostly accepted FeSC pairing state [41,42]. However, the multiband character of FeSCs also offers chances for more exotic pairing states [39,42], and thus we will also discuss TE properties with other order-parameter symmetries in the following. Hereinafter, we take the interorbital hopping parameter $|t_1|$ as a standard unit of energy, and temperature is measured in units of $|t_1|/k_{\rm B}$ [43]. Finally, the FeSC total DoS turns out to be the sum of an electronlike [+, blue curve in Fig. 1(b)] and a holelike [−, red curve in Fig. 1(b)] band contribution [44], $\mathcal{N}_{\rm FeSC}(\varepsilon) = \mathcal{N}^+_{\rm FeSC}(\varepsilon) + \mathcal{N}^-_{\rm FeSC}(\varepsilon)$, where

$$\mathcal{N}^{\pm}_{\rm FeSC}(\varepsilon) = \sum_{\mathbf{k}}\frac{\varepsilon + \varepsilon^0_{\mathbf{k}\pm}}{2\varepsilon^d_{\mathbf{k}\pm}}\left\{\delta\left[\varepsilon^d_{\mathbf{k}\pm} - \varepsilon\right] - \delta\left[\varepsilon^d_{\mathbf{k}\pm} + \varepsilon\right]\right\}. \tag{4}$$

Note also that the superconducting instability opens the gap symmetrically around the chemical potential, as illustrated in the inset of Fig. 1(b) (see also the Supplemental Material [40]).

Figures of merit. In order to quantify the TE performance, it is usual to consider the Seebeck coefficient $S = -\alpha/(\sigma T)$ and thermodynamic efficiency with the dimensionless figure of merit ${\rm ZT} = S^2\sigma T/[\kappa - \alpha^2/(\sigma T)]$ [45]. A large value of ZT means better thermodynamic efficiency, and if it tends to infinity, the efficiency of the device tends to the Carnot limit. In the following, we show how S and ZT of an FeSC–insulator–normal-metal (FeSC-I-N) junction depend on the temperature, considering possible different values of $\Delta_0^{\rm FeSC}$ [46] and changing the doping level, μ [47].

Figures 2(a) and 2(b) collect the $S(T, \Delta_0^{\rm FeSC})$ and ${\rm ZT}(T, \Delta_0^{\rm FeSC})$ maps at the half-filling condition $\mu = 1.54$. For a given $\Delta_0^{\rm FeSC}$, both the Seebeck coefficient and the TE efficiency behave nonmonotonically, with a clear maximum that shifts towards gradually higher temperatures as $\Delta_0^{\rm FeSC}$ increases. Indeed, $\Delta_0^{\rm FeSC}$ is the energy scale that mainly influences the optimal temperature that maximizes the TE effect. Furthermore, by increasing $\Delta_0^{\rm FeSC}$ the subgap states reduce, correspondingly requiring higher energies to achieve the same TE effect. The use of FeSCs is a further advantage over conventional SC configurations, since it allows operation at higher temperatures that provide a larger Seebeck coefficient.

Figures 2(c) and 2(d) show what happens when changing the doping level, keeping fixed $\Delta_0^{\rm FeSC} = 0.1$ [48]. The FeSC DoS dependence on μ is illustrated in the Supplemental Material [40]. The $S(T, \mu)$ map still reveals single-peaked profiles, but modifying the doping we observe the inversion of the Seebeck coefficient sign around $\mu \sim 0.75$, below (above) which $S > 0$ ($S < 0$) for the hole (electron) DoS contribution dominates. We note that the point at which the Seebeck coefficient changes sign differs from the half-filling condition. The reason for this is the lack of symmetry between particlelike and holelike bands for an FeSC in the energy window determined by the working temperatures.

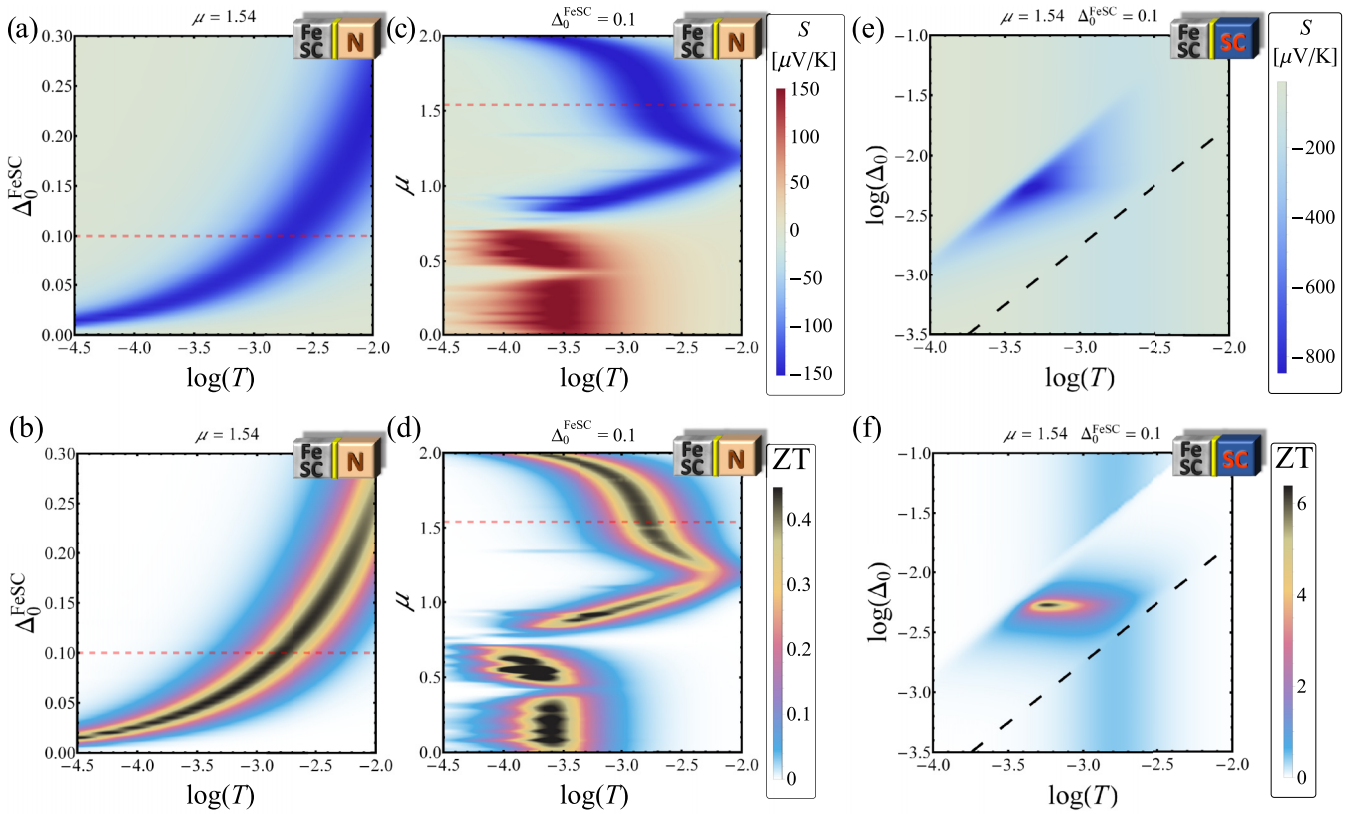

FIG. 2. FeSC-I-N junction: (a) and (b) Seebeck coefficient, $S(T, \Delta_0^{\rm FeSC})$, and figure of merit, $\mathrm{ZT}(T, \Delta_0^{\rm FeSC})$ at $\mu = 1.54$. (c) and (d) $S(T, \mu)$ and $\mathrm{ZT}(T, \mu)$, at $\Delta_0^{\rm FeSC} = 0.1$. The legends in (c) and (d) refer also to (a) and (b), respectively, and the red dashed line marks the condition $(\Delta_0^{\rm FeSC}, \mu) = (0.1, 1.54)$. FeSC-I-S junction: (e) and (f) $S(T, \Delta_0)$ and $\mathrm{ZT}(T, \Delta_0)$, at $\mu = 1.54$, $\Delta_0^{\rm FeSC} = 0.1$, and $\gamma = 10^{-4}$. The dashed lines in (c) and (f) mark the values $\Delta_0^{th} = 1.764T$. A cartoon in the top-right corner of each panel helps the reader to recognize the type of junction considered at a glance.

In the cases discussed so far, we achieve Seebeck coefficients up to $|S| \sim 150$ μV/K reaching also TE efficiencies of $\mathrm{ZT} \sim 0.5$. In the case of an undoped FeSC, $\mu = 1.54$, with $\Delta_0^{\rm FeSC} = 0.1$, i.e., the red dashed lines in Figs. 2(a)–2(d), the highest TE efficiency is reached at $T \simeq 1.6 \times 10^{-3}$, which may be a temperature around 2.8 K.

We remark that the maximum Seebeck coefficient we obtain is several orders of magnitude larger than that usually found in metallic structures at the same temperatures. However, in terms of the thermoelectricity, the FeSC-I-N junction outperforms magnetic TJs [49] and is quite well comparable to hybrid SC-ferromagnet TJs [50,51] and quantum-dot setups [52].

It is noteworthy to show that if we replace the normal metal with a BCS SC with a gap Δ_0, the linear thermoelectricity can be further enhanced. This effect can be ascribed to the additional contribution of the conventional DoS peaks intertwined with the multiband character of the FeSC. Thus, in Figs. 2(e) and 2(f), we present the $S(T, \Delta_0)$ and $\mathrm{ZT}(T, \Delta_0)$ maps of an FeSC-insulator-SC (FeSC-I-S) TJ. In this case, we assume a specific FeSC with a given gap $\Delta_0^{\rm FeSC} = 0.1$, and we explore the TE response at different values of the BCS superconducting gap Δ_0. A region of the (T, Δ_0) parameter space emerges in which both the Seebeck coefficient and the TE efficiency increase significantly, even reaching the values $|S| \sim 870$ μV/K and $\mathrm{ZT} \sim 6.5$ at $(T, \Delta_0)_{\rm max} \simeq (0.63, 5.3) \times 10^{-3}$. In natural units, these quantities correspond to $T \simeq 1.8$ K for a BCS SC with $T_c \simeq 5.2$ K [53].

Order-parameter symmetry detection. We show here that TE figures of merit are also a powerful tool for addressing order-parameter symmetry (OPS). We compare the temperature dependence of S and ZT of an FeSC-I-N TJ, with $\mu = 1.54$ and $\Delta_0^{\rm FeSC} = 0.1$, taking into account different OPSs: We cover the three possible s-wave symmetries, i.e., the constant-gap case s_0, $s_{x^2y^2} = \Delta_0^{\rm FeSC} \cos k_x \cos k_y$, and $s_{x^2+y^2} = \Delta_0^{\rm FeSC}(\cos k_x + \cos k_y)/2$, and the two d-wave symmetries, i.e., $d_{xy} = \Delta_0^{\rm FeSC} \sin k_x \sin k_y$ and $d_{x^2-y^2} = \Delta_0^{\rm FeSC}(\cos k_x - \cos k_y)/2$ [54]. Since it will be useful later on, we recall that the $d_{x^2-y^2}$, d_{xy}, and $s_{x^2+y^2}$ OPSs are nodal, while the others are nodeless [39,55].

Figure 3 demonstrates that the TE figures of merit can provide valuable clues for determining the OPS of the system. Figure 3(a) takes a closer look at the different DoSs in play, with the inset serving to highlight the low-energy region. Figures 3(b) and 3(c) illustrate the Seebeck coefficient $S(T)$ and the TE efficiency $\mathrm{ZT}(T)$, both showing, on a semilog scale, bell-shaped, single-peaked profiles for each symmetry considered. It immediately stands out that the "position" of these peaks depends strongly on the OPS: Indeed, for the s_0 and $s_{x^2y^2}$ cases, both S and ZT are peaked roughly around $T^{\rm peak} \sim 10^{-3}$, while the other symmetries give S and ZT peaks centered on temperatures an order of

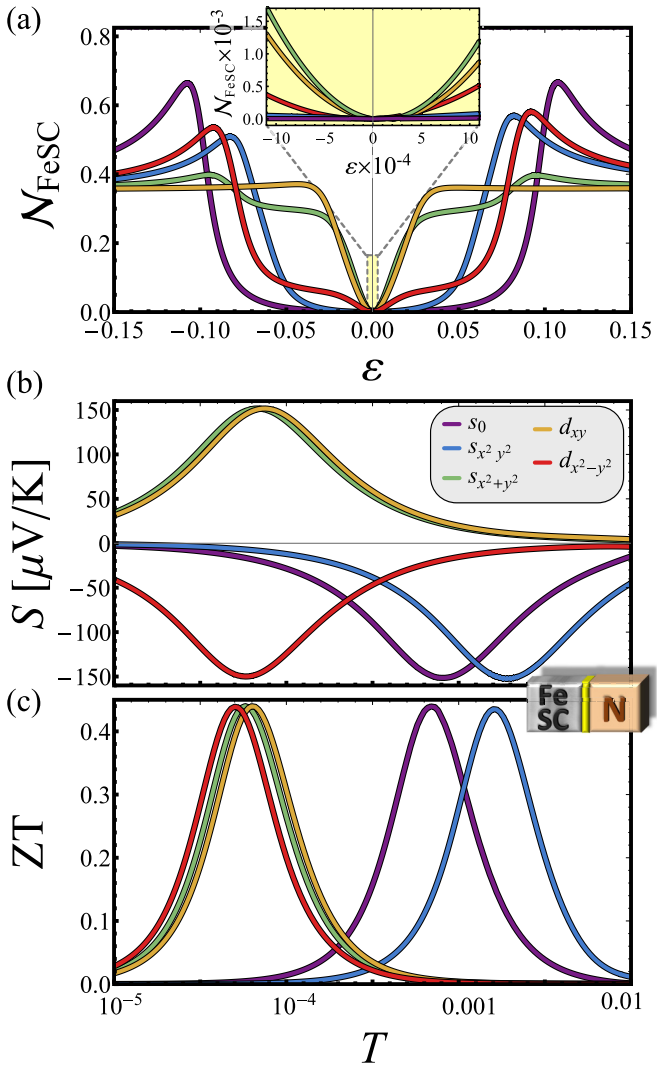

FIG. 3. FeSC-I-N junction: (a) DoS, $\mathcal{N}_{\rm FeSC}(\varepsilon)$; (b) Seebeck coefficient, $S(T)$; and (c) figure of merit, $\mathrm{ZT}(T)$, for different symmetries of the order parameter, at $\mu = 1.54$ and $\Delta_0^{\rm FeSC} = 0.1$. The inset in (a) illustrates the low-energy behavior of the DoSs. The legend in (b) refers to all panels.

magnitude lower. To give realistic numbers (here the subscript distinguishes symmetries), the S peaks for nodeless OPSs are located at $T_{x^2y^2}^{\rm peak} \simeq 3.3$ K (blue) and $T_0^{\rm peak} \simeq 1.4$ K (violet), whereas for nodal cases one finds $T_{xy}^{\rm peak} \simeq 0.13$ K (yellow), $T_{x^2+y^2}^{\rm peak} \simeq 0.12$ K (green), and $T_{x^2-y^2}^{\rm peak} \simeq 0.10$ K (red). To grasp this result, we recall that the energy window relevant for calculating the TE coefficients scales with temperature, i.e., $|\varepsilon| \sim T$ [40]. For instance, the energies considered in the inset of Fig. 3(a) are essentially those where one should focus if $T \sim 10^{-4}$. Here, it is evident that only the d_{xy}, $s_{x^2+y^2}$, and $d_{x^2-y^2}$ DoSs (i.e., those showing ZTs peaked at these temperatures) are clearly nonzero. We see that nodeless FeSC pairings present maximal thermoelectricity (absolute value of the Seebeck coefficient) at relatively high temperatures. Instead, for the nodal cases, due to the presence of low-energy states in the gap, the maximal thermoelectricity is observed at much lower temperature regimes. This result is quite robust in the presence of variations in the gap amplitude, hopping parameter, and chemical potential values [40]. Furthermore, we also see that the first two DoSs, i.e., the yellow and green curves, are unbalanced toward the hole side ($\varepsilon < 0$), unlike the third DoS, i.e., the red curve, which appears to be slightly unbalanced toward the particle side ($\varepsilon > 0$). This is directly reflected in the sign of S, which immediately tells us the PH asymmetry of the FeSC DoS, and therefore $S > 0$ ($S < 0$) in the former (latter) case. This is clearly confirmed also by looking at the PH asymmetry of the DoSs on the larger energy scale considered in Fig. 3(a). It is evident, for instance, that the s_0 and $s_{x^2y^2}$ OPSs, i.e., the violet and blue curves, respectively, are unbalanced to the right, i.e., the particle contribution dominates, thereby making S negative.

We emphasize that in principle, the measurement of the PH asymmetry could be addressed by directly measuring the tunneling differential conductance. However, a systematic experimental asymmetry in the bias polarization of the junction cannot be easily excluded thus loosing sensitivity for small PH asymmetry. The linear thermoelectricity much more safely returns this information in an independent way. Yet we stress that the thermoelectrical signatures discussed in this Research Letter, being associated with the quasiparticle tunneling in the junction, are not affected by any phonon- or magnon-drag effects, which instead usually influence the bulk TE properties in the normal phase [27].

Conclusions. To summarize, we have demonstrated that an FeSC TJ can show sizable TE efficiency and that both the TE figure of merit and the Seebeck coefficient are found to be nonmonotonic, single-peaked functions of temperature. Moreover, they can provide details of the underlying symmetry of the order parameter addressing the PH asymmetry of the DoS. In particular, we demonstrated in an FeSC-I-N junction that the position of both the ZT and S peaks allows us to clearly distinguish nodal from nodeless symmetries. Furthermore, the sign of S provides further information about the PH asymmetry, distinguishing cases where the TE efficiency is not discriminating, such as for the two d-wave symmetries. Our results also establish the relevance of multiband SCs forthe generation of novel TE devices.

As a closing remark, we observe that the proposed approach may be used for studying other quantum materials [42]. Multiorbital pairing approaches have been widely used also to shed light on other multiband SCs, such as ruthenates and nickelates, and to provide insights into Hund metals. Therefore the TE-based investigation of tunnel junctions presented in this Research Letter complements the actual experimental techniques, providing fertile ground for the study of novel quantum materials.

Acknowledgments. F.G. acknowledges PNRR MUR Project No. PE0000023-NQSTI for partial financial support. F.G. and A.B. acknowledge the EU's Horizon 2020 research and innovation program under Grant Agreements No. 964398 (SUPERGATE) and No. 101057977 (SPECTRUM) for partial financial support. A.B. acknowledges PRIN2022 PNRR MUR project NEThEQS (Grant No. 2022B9P8LN) and the Royal Society through the International Exchanges Scheme between the UK and Italy (Grants No. IEC R2 192166.) for partial financial support. R.C. acknowledges the project HORIZON-EIC-2022-PATHFINDERCHALLENGES-01 GA N.101115190 – IQARO.

[1] A. Fornieri and F. Giazotto, Towards phase-coherent caloritronics in superconducting circuits, Nat. Nanotechnol. **12**, 944 (2017).

[2] S.-Y. Hwang and B. Sothmann, Phase-coherent caloritronics with ordinary and topological Josephson junctions, Eur. Phys. J. Spec. Top. **229**, 683 (2020).

[3] F. Giazotto, T. T. Heikkilä, A. Luukanen, A. M. Savin, and J. P. Pekola, Opportunities for mesoscopics in thermometry and refrigeration: Physics and applications, Rev. Mod. Phys. **78**, 217 (2006).

[4] J. T. Muhonen, M. Meschke, and J. P. Pekola, Micrometre-scale refrigerators, Rep. Prog. Phys. **75**, 046501 (2012).

[5] A. Ozaeta, P. Virtanen, F. S. Bergeret, and T. T. Heikkilä, Predicted Very Large Thermoelectric Effect in Ferromagnet-Superconductor Junctions in the Presence of a Spin-Splitting Magnetic Field, Phys. Rev. Lett. **112**, 057001 (2014).

[6] S. Kolenda, M. J. Wolf, and D. Beckmann, Observation of Thermoelectric Currents in High-Field Superconductor-Ferromagnet Tunnel Junctions, Phys. Rev. Lett. **116**, 097001 (2016).

[7] F. S. Bergeret, M. Silaev, P. Virtanen, and T. T. Heikkilä, Colloquium: Nonequilibrium effects in superconductors with a spin-splitting field, Rev. Mod. Phys. **90**, 041001 (2018).

[8] R. Hussein, M. Governale, S. Kohler, W. Belzig, F. Giazotto, and A. Braggio, Nonlocal thermoelectricity in a Cooper-pair splitter, Phys. Rev. B **99**, 075429 (2019).

[9] G. Marchegiani, A. Braggio, and F. Giazotto, Nonlinear Thermoelectricity with Electron-Hole Symmetric Systems, Phys. Rev. Lett. **124**, 106801 (2020).

[10] G. Blasi, F. Taddei, L. Arrachea, M. Carrega, and A. Braggio, Nonlocal Thermoelectricity in a Superconductor–Topological-Insulator–Superconductor Junction in Contact with a Normal-Metal Probe: Evidence for Helical Edge States, Phys. Rev. Lett. **124**, 227701 (2020).

[11] G. Blasi, F. Taddei, L. Arrachea, M. Carrega, and A. Braggio, Nonlocal thermoelectricity in a topological Andreev interferometer, Phys. Rev. B **102**, 241302(R) (2020).

[12] G. Germanese, F. Paolucci, G. Marchegiani, A. Braggio, and F. Giazotto, Bipolar thermoelectric Josephson engine, Nat. Nanotechnol. **17**, 1084 (2022).

[13] F. Giazotto, P. Solinas, A. Braggio, and F. S. Bergeret, Ferromagnetic-Insulator-Based Superconducting Junctions as Sensitive Electron Thermometers, Phys. Rev. Appl. **4**, 044016 (2015).

[14] T. T. Heikkilä, R. Ojajärvi, I. J. Maasilta, E. Strambini, F. Giazotto, and F. S. Bergeret, Thermoelectric Radiation Detector Based on Superconductor-Ferromagnet Systems, Phys. Rev. Appl. **10**, 034053 (2018).

[15] F. Paolucci, G. Germanese, A. Braggio, and F. Giazotto, A highly sensitive broadband superconducting thermoelectric single-photon detector, Appl. Phys. Lett. **122**, 173503 (2023).

[16] P. Machon, M. Eschrig, and W. Belzig, Giant thermoelectric effects in a proximity-coupled superconductor–ferromagnet device, New J. Phys. **16**, 073002 (2014).

[17] G. Goll, *Unconventional Superconductors: Experimental Investigation of the Order-Parameter Symmetry of Unconventional Superconductors* (Springer, Berlin, 2006).

[18] J.-P. Reid, M. A. Tanatar, A. Juneau-Fecteau, R. T. Gordon, S. R. de Cotret, N. Doiron-Leyraud, T. Saito, H. Fukazawa, Y. Kohori, K. Kihou, C. H. Lee, A. Iyo, H. Eisaki, R. Prozorov, and L. Taillefer, Universal Heat Conduction in the Iron Arsenide Superconductor KFe_2As_2: Evidence of a *d*-Wave State, Phys. Rev. Lett. **109**, 087001 (2012).

[19] *The Iron Pnictide Superconductors: An Introduction and Overview*, edited by F. Mancini and R. Citro (Springer, Cham, Switzerland, 2017).

[20] C. Benjamin and T. Mohapatra, Shot noise as a probe for the pairing symmetry of iron pnictide superconductors, Europhys. Lett. **132**, 47002 (2020).

[21] I. I. Mazin, D. J. Singh, M. D. Johannes, and M. H. Du, Unconventional Superconductivity with a Sign Reversal in the Order Parameter of $LaFeAsO_{1-x}F_x$, Phys. Rev. Lett. **101**, 057003 (2008).

[22] F. Wang, H. Zhai, Y. Ran, A. Vishwanath, and D.-H. Lee, Functional Renormalization-Group Study of the Pairing Symmetry and Pairing Mechanism of the FeAs-Based High-Temperature Superconductor, Phys. Rev. Lett. **102**, 047005 (2009).

[23] C. Guarcello and R. Citro, Progresses on topological phenomena, time-driven phase transitions, and unconventional superconductivity, Europhys. Lett. **132**, 60003 (2020).

[24] K. Kuroki, S. Onari, R. Arita, H. Usui, Y. Tanaka, H. Kontani, and H. Aoki, Unconventional Pairing Originating from the Disconnected Fermi Surfaces of Superconducting $LaFeAsO_{1-x}F_x$, Phys. Rev. Lett. **101**, 087004 (2008).

[25] T. Chen, Z. Tesanovic, R. Liu, X. Chen, and C. Chien, A BCS-like gap in the superconductor $SmFeAsO_{0.85}F_{0.15}$, Nature (London) **453**, 1224 (2008).

[26] D. Daghero, M. Tortello, G. Ummarino, V. Stepanov, F. Bernardini, M. Tropeano, M. Putti, and R. Gonnelli, Effects of isoelectronic Ru substitution at the Fe site on the energy gaps of optimally F-doped SmFeAsO, Supercond. Sci. Technol. **25**, 084012 (2012).

[27] I. Pallecchi, F. Caglieris, and M. Putti, Thermoelectric properties of iron-based superconductors and parent compounds, Supercond. Sci. Technol. **29**, 073002 (2016).

[28] J. M. Ziman, *Electrons and Phonons: The Theory of Transport Phenomena in Solids* (Oxford University Press, Oxford, 2001).

[29] F. Caglieris, A. Braggio, I. Pallecchi, A. Provino, M. Pani, G. Lamura, A. Jost, U. Zeitler, E. Galleani D'Agliano, P. Manfrinetti, and M. Putti, Magneto-Seebeck effect in *R*FeAsO (R = rare earth) compounds: Probing the magnon drag scenario, Phys. Rev. B **90**, 134421 (2014).

[30] G. Germanese, F. Paolucci, G. Marchegiani, A. Braggio, and F. Giazotto, Superconducting bipolar thermoelectric memory and method for writing a superconducting bipolar thermo-electric memory, I.T. Patent No. 102021000032042 (2021).

[31] G. Germanese, F. Paolucci, A. Braggio, and F. Giazotto, Broadband passive superconducting thermoelectric single photon-detector, I.T. Patent No. 102023000001854 (2023).

[32] G. Benenti, G. Casati, K. Saito, and R. Whitney, Fundamental aspects of steady-state conversion of heat to work at the nanoscale, Phys. Rep. **694**, 1 (2017).

[33] R. C. Dynes, V. Narayanamurti, and J. P. Garno, Direct Measurement of Quasiparticle-Lifetime Broadening in a Strong-Coupled Superconductor, Phys. Rev. Lett. **41**, 1509 (1978).

[34] C. Guarcello, A. Braggio, P. Solinas, and F. Giazotto, Nonlinear Critical-Current Thermal Response of an Asymmetric

Josephson Tunnel Junction, Phys. Rev. Appl. **11**, 024002 (2019).

[35] C. Guarcello, A. Braggio, P. Solinas, G. P. Pepe, and F. Giazotto, Josephson-Threshold Calorimeter, Phys. Rev. Appl. **11**, 054074 (2019).

[36] This can be done using different strategies such as increasing the barrier opacity or using superconducting quantum interference device (SQUID)-like interference or even Fraunhofer-like suppression [9,12].

[37] S. Raghu, X.-L. Qi, C.-X. Liu, D. J. Scalapino, and S.-C. Zhang, Minimal two-band model of the superconducting iron oxypnictides, Phys. Rev. B **77**, 220503(R) (2008).

[38] Our goal is to understand the influence of multiband superconductivity on TE properties; thus Raghu *et al.*'s approach [37] is sufficient, although we are aware that models with more orbitals have also been developed [56,57] and are often used to investigate multiband effects on superconductivity and magnetism in FeSC materials [58,59].

[39] M. M. Parish, J. Hu, and B. A. Bernevig, Experimental consequences of the s-wave $\cos(k_x)\cos(k_y)$ superconductivity in the iron pnictides, Phys. Rev. B. **78**, 144514 (2008).

[40] See Supplemental Material at http://link.aps.org/supplemental/10.1103/PhysRevB.108.L100511 for the details of the model used for describing FeSCs, details of the FeSC DoS; the calculation of linear TE coefficients in the cases discussed in Fig. 2, the calculation of TE effects in the case of other OPSs, the robustness of TE effects in the presence of chemical potential variations, the calculation of the power factor, and the relation between the superconducting gaps at the optimal TE efficiency. The Supplemental Material also contains Refs. [60–62].

[41] Y. Bang and G. R. Stewart, Superconducting properties of the $s^{\pm}$-wave state: Fe-based superconductors, J. Phys.: Condens. Matter **29**, 123003 (2017).

[42] R. M. Fernandes, A. I. Coldea, H. Ding, I. R. Fisher, P. J. Hirschfeld, and G. Kotliar, Iron pnictides and chalcogenides: A new paradigm for superconductivity, Nature (London) **601**, 35 (2022).

[43] Hereinafter, we assume an interorbital hopping parameter $|t_1| = 0.15$ eV, in line with the values often used in the literature, e.g., Ref. [63].

[44] A. Ptok, Influence of $s_{\pm}$ symmetry on unconventional superconductivity in pnictides above the Pauli limit–two-band model study, Eur. Phys. J. B **87**, 2 (2014).

[45] For a complete TE characterization of the device, it is required also to look at the power that the system produces as an energy harvester, which is quantified by the *power factor*, $\mathrm{PF} = \sigma S^2$ [32]. More details and the specific calculation of PF in the cases of interest for the present work are reported in the Supplemental Material [40].

[46] FeSCs have been found to exhibit a wide range of superconducting transition temperatures [42], albeit the $2\Delta_{\max}/(k_{\mathrm{B}}T_c)$ ratio (with $\Delta_{\max}$ being the zero-temperature value of the largest gap) often falls within 6.0–8.5, in contrast to the ∼3.5 value of conventional BCS SCs.

[47] In this Research Letter we are assuming a temperature-independent gap because we typically consider temperatures $T < 0.4T_c$ since the FeSC superconductive gap shows a BCS-like temperature dependence [64].

[48] The value $\Delta_0^{\mathrm{FeSC}} = 0.1$, hereinafter used in this Research Letter, corresponds to $T_c \in [41–58]$ K.

[49] M. Walter, J. Walowski, V. Zbarsky, M. Münzenberg, M. Schäfers, D. Ebke, G. Reiss, A. Thomas, P. Peretzki, M. Seibt, J. S. Moodera, M. Czerner, M. Bachmann, and C. Heiliger, Seebeck effect in magnetic tunnel junctions, Nat. Mater. **10**, 742 (2011).

[50] S. Kolenda, C. Sürgers, G. Fischer, and D. Beckmann, Thermoelectric effects in superconductor-ferromagnet tunnel junctions on europium sulfide, Phys. Rev. B **95**, 224505 (2017).

[51] C. González-Ruano, D. Caso, J. A. Ouassou, C. Tiusan, Y. Lu, J. Linder, and F. G. Aliev, Observation of Magnetic State Dependent Thermoelectricity in Superconducting Spin Valves, Phys. Rev. Lett. **130**, 237001 (2023).

[52] A. Svilans, M. Leijnse, and H. Linke, Experiments on the thermoelectric properties of quantum dots, C. R. Phys. **17**, 1096 (2016).

[53] We included in Figs. 2(e) and 2(f) a black dashed line to mark the condition $T = T_c$ at which the noniron electrode ceases to be superconductive and the system actually behaves as an FeSC-I-N junction. Figure 2(f) allows us also to investigate the functional dependence existing between the superconducting gaps in the region of parameter space that gives the optimal TE efficiency [40].

[54] Raghu *et al.*'s approach [37] entails two pairing gaps, one for each orbital, $\Delta_{1,2}$, that satisfy the condition $\Delta_1(k_x, k_y) = \Delta_2(k_y, k_x)$ for all the pairing symmetries described above, except for $d_{x^2-y^2}$ giving $\Delta_1(k_x, k_y) = -\Delta_2(k_x, k_y)$ [39,55]. In the latter case, the eigenvalues and the DoSs are not reduced to the simple expressions given in Eqs. (3) and (4), but we use the general expression of the spectral function given in Ref. [39] with the eigenvalues presented in Ref. [55].

[55] K. Seo, B. A. Bernevig, and J. Hu, Pairing Symmetry in a Two-Orbital Exchange Coupling Model of Oxypnictides, Phys. Rev. Lett. **101**, 206404 (2008).

[56] H. Eschrig and K. Koepernik, Tight-binding models for the iron-based superconductors, Phys. Rev. B **80**, 104503 (2009).

[57] E. M. Nica, R. Yu, and Q. Si, Orbital-selective pairing and superconductivity in iron selenides, npj Quantum Mater. **2**, 24 (2017).

[58] J. Querales Flores, C. Ventura, R. Citro, and J. Rodríguez-Núñez, Temperature and doping dependence of normal state spectral properties in a two-orbital model for ferropnictides, Phys. Lett. A **380**, 1648 (2016).

[59] D. C. Cavanagh and P. M. R. Brydon, General theory of robustness against disorder in multiband superconductors, Phys. Rev. B **104**, 014503 (2021).

[60] H. Yamase and R. Zeyher, Superconductivity from orbital nematic fluctuations, Phys. Rev. B **88**, 180502(R) (2013).

[61] P. T. Dumitrescu, M. Serbyn, R. T. Scalettar, and A. Vishwanath, Superconductivity and nematic fluctuations in a model of doped FeSe monolayers: Determinant quantum Monte Carlo study, Phys. Rev. B **94**, 155127 (2016).

[62] G. Liu, S. Fang, X. Zheng, Z. Huang, and H. Lin, Interplay between nematic fluctuation and superconductivity in a two-orbital Hubbard model: a quantum Monte Carlo study, J. Phys.: Condens. Matter **30**, 445604 (2018).

[63] Z. Wang and A. H. Nevidomskyy, Orbital nematic order and interplay with magnetism in the two-orbital Hubbard model, J. Phys.: Condens. Matter **27**, 225602 (2015).

[64] R. Jin, M. H. Pan, X. B. He, G. Li, D. Li, R. wen Peng, J. R. Thompson, B. C. Sales, A. S. Sefat, M. A. McGuire, D. Mandrus, J. F. Wendelken, V. Keppens, and E. W. Plummer, Electronic, magnetic and optical properties of two Fe-based superconductors and related parent compounds, Supercond. Sci. Technol. **23**, 054005 (2010).